ICANS XIX,
19th meeting on Collaboration of Advanced Neutron Sources
March 8 – 12, 2010
Grindelwald, Switzerland

The Effect of Gas Bubble Injection for Pressure Wave Mitigation in High-Power Neutron Sources – Differences and Similarities between Mercury and Water

Masato IDA, Takashi NAOE, and Masatoshi FUTAKAWA
J-PARC Center, Japan Atomic Energy Agency,
2-4 Shirakata-Shirane, Tokai-mura, Naka-Gun, Ibaraki 319-1195, Japan

ABSTRACT

Gas bubble injection into liquid mercury is one of the techniques that we have attempted to mitigate intense pressure waves induced by proton injection into liquid-mercury targets. We are now at the stage of verification of its true effect in a realistic condition. However, detailed experimental examination of the technique in liquid mercury poses great challenges: The opacity of mercury, among other factors, hinders us from a fine observation of the events occurring in the bubbly liquid. From this reason, we are performing alternative experiments using a clear liquid, water, in conjunction with mercury experiments. In this talk, we discuss numerically and theoretically the differences and similarity in the bubble injection effects in mercury and water to evaluate the validity and usefulness of the water experiment. The present result reveals an important similarity between mercury and water, which supports the usefulness of water experiment. We also report our recent result of a water experiment which clearly demonstrates the significant effect of gas microbubbles.

1. Introduction: Proton-Induced Cavitation Damage and Gas Bubble Injection

Proton-induced cavitation damage is now a significant issue in developing high-power neutron sources using liquid mercury. Abrupt heating of mercury due to the injection of high-energy proton beams radiates intense pressure waves and they induce cavitation of mercury. The cavitation bubbles emerging through the cavitation process expand explosively and then collapse violently to cause significant damages on the flow vessels.

Gas bubble injection is a promising technique to mitigate cavitation damage. From the previous theoretical and numerical studies [1–5], the effect of this technique has been thoroughly clarified. Now we know that gas microbubbles have three favorable functions: (a) the absorption effect to reduce the pressure rise of mercury induced by proton injection; (b) the attenuation effect to damp the pressure waves propagating in mercury; and (c) the suppression effect to suppress the inception of cavitation. Our recent focus was on verifying and realizing these functions by experiment.

In performing laboratory experiments with mercury, a number of difficulties arise. The most significant one comes from the opacity of mercury. Due to its silver colour, one cannot see by optical techniques what takes place inside mercury. From this reason, we have performed alternative experiments with a clear liquid, water, in conjunction with mercury experiments. Water is useful not only because of its transparency but also because of its safety. However, water is much different from liquid mercury in many respects and hence one has to be careful in using the result with water. From previous investigations,

we actually found that the rise velocity of bubbles and the eigenfrequency of *single bubbles*, for example, are much different in water and mercury.

However, we recently found numerically that the responses of bubbly water and bubbly mercury to rapid heat input are, in some cases, very similar to each other [6]. We revealed theoretically that this unexpected similarity comes from a similarity between *bubble clouds* in water and mercury. This similarity allows one to estimate the case of mercury from results obtained using water. In the following sections, we review the discovered similarity and its consequences. We also report some important results from a water experiment performed recently using high-voltage spark discharges.

2. Numerical Demonstration of a Similarity between Bubble Clouds in Water and Mercury

To clearly demonstrate the similarity between bubble clouds in water and mercury, we investigate the absorption effect of microbubbles. As demonstrated theoretically and numerically [1, 2, 4], gas microbubbles can significantly reduce the amplitude of the proton-induced pressure waves. The origin of this effect is the high compressibility of the gas in the bubbles. When the heat release due to proton injection occurs, liquid mercury tends to undergo rapid thermal expansion and its pressure begins to rise rapidly. When gas microbubbles are suspended within the spallation region, mercury can easily expand and the pressure rise is thus decreased. This effect is what we call the absorption effect. Because the time scale of the energy release is very short in the real targets, a smaller bubble, having a higher eigenfrequency, can have a stronger absorption effect [4].

Since the eigenfrequency of a single bubble is proportional to $1/\sqrt{\rho}$ with ρ being the liquid density, a single bubble in water has a much higher (about 3.7 times) eigenfrequency than that in mercury. This large difference appears to lead to a significant difference in bubble dynamics and the absorption effect. We discussed this possibility by using a direct numerical simulation (DNS) method [4]. In this method, equations for liquid flow and a bubble dynamics equation are coupled through the void fraction of bubbles, liquid pressure, and thermal conduction. Using this method and assuming the liquid to be water, we reconsidered the problem studied in Ref. [4], that is, response of a bubbly liquid to rapid heat input. The result with water was compared to that with mercury.

The flow field is assumed to be a straight cylinder filled with a bubbly liquid, and symmetry is assumed in the axial and azimuthal directions. Hereafter, subscripts "*L*" and "*G*" denote quantities for the liquid and the gas in the bubbles, respectively. The equations for liquid flow are the mass, momentum, and energy conservation equations for dilute bubbly liquids:

$$\frac{D_L f_L \rho_L}{Dt} + f_L \rho_L \frac{1}{r}\frac{\partial r u_L}{\partial r} = 0, \tag{1}$$

$$f_L \rho_L \frac{D_L u_L}{Dt} = -\frac{\partial p}{\partial r} + \frac{1}{r}\frac{\partial}{\partial r}\left\{\frac{4}{3}\mu_e\left(\frac{1}{r}\frac{\partial r u_L}{\partial r}\right)\right\}, \tag{2}$$

$$f_L \rho_L C_{pL} \frac{D_L T_L}{Dt} = f_L \beta_L T_L \frac{D_L p}{Dt} + \frac{1}{r}\frac{\partial}{\partial r}\left(r f_L \lambda_L \frac{\partial T_L}{\partial r}\right) + Q, \tag{3}$$

where $D_L / Dt \equiv \partial / \partial t + u_L \partial / \partial r$, ρ_L is the liquid density, f_L is the liquid volume fraction, u_L is the velocity, p the pressure, C_{pL} the isobaric heat capacity, T_L the temperature, β_L the coefficient of thermal expansion, λ_L the thermal conductivity, Q the heat input due to the energy release, r the radial coordinate. The effective viscosity μ_e is determined by $\mu_e = (1 + 2.5 f_G)\mu_L$ with the gas volume fraction f_G and the liquid viscosity μ_L.

The bubble dynamics equation is based on the Keller equation:

$$\left(1 - \frac{\dot{R}}{c_L}\right) R\ddot{R} + \left(\frac{3}{2} - \frac{\dot{R}}{2c_L}\right)\dot{R}^2 = \frac{1}{\rho_L}\left(1 + \frac{\dot{R}}{c_L}\right) p_d + \frac{R}{\rho_L c_L}\dot{p}_d, \tag{4}$$

$$p_d = p_G - \frac{2\sigma}{R} - \frac{4\mu_L \dot{R}}{R} - p, \tag{5}$$

where the overdot denotes time derivative, $R = R(t)$ is the instantaneous radius of the bubble, c_L is the sound speed of the liquid at the bubble surface, and σ is the surface tension. This equation governs the time evolution of the radius of a spherical bubble driven by the change in liquid pressure p. The bubble content is assumed to be an ideal gas and the gas pressure p_G is determined by solving the mass, momentum, and energy conservation equations for gas flows [4]. To close this system, the equation of state (EOS) of the liquid is needed. The EOS used here for water is the Tait equation, $(p + B)/(p_0 + B) = (\rho_L / \rho_{L,0})^{7.15}$, where $B = 308$ MPa, p_0 is the atmospheric pressure, and $\rho_{L,0}$ is the liquid density at $p = p_0$. Although B is known to depend on temperature, we assume it to be constant because the temperature change observed in our computation was only 6 K at most. The fluid equations are solved by a finite difference method and the Keller equation is solved by a Runge-Kutta method. The volume fractions are calculated using the number density of bubbles, n_b, and R. Assuming that all bubbles in a computational cell are identical and have the same dynamics, the Keller equation is solved once per time step in each cell. See Ref. [4] for further details of this DNS method and the governing equations.

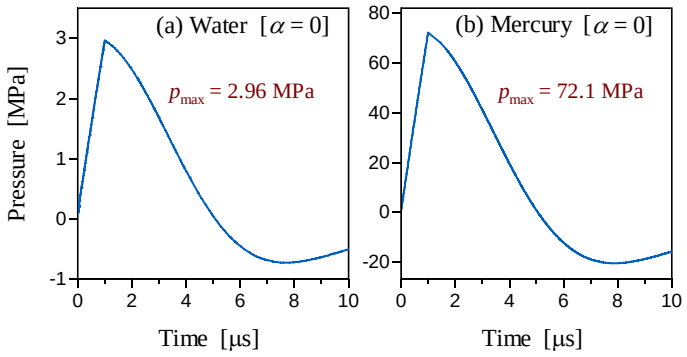

Fig. 1. Pressure-time curves at the cylinder center for (a) water and (b) mercury with $\alpha = 0$.

The radius of the computational space is 30 mm and 200 grid points are used to resolve it. At $t = 0$, $\rho_L = 1000\,\mathrm{kg/m^3}$, $u_L = 0\,\mathrm{m/s}$, $p = 0.1\mathrm{MPa}$, and $T_L = 323.15\,\mathrm{K}$ and they are spatially uniform. The heat input Q has a Gaussian distribution in space and is assumed here as

$$Q(t) = \begin{cases} \chi Q_{\max} \exp(-r^2 / 2\phi^2) & \text{for } 0 \le t \le 1\,\mu\mathrm{s}, \\ 0 & \text{otherwise}, \end{cases} \qquad (6)$$

where $Q_{\max} = 26.7 \times 10^{12}\ \mathrm{W/m^3}$ and $\phi = 5$ mm. χ is a free parameter to control the magnitude of Q: for $\chi = 1$, Eq. (6) comes to be the same as that used in Ref. [4]. The bubble content is assumed to be helium. We assume that all bubbles are identical and initially at equilibrium and n_b is spatially uniform. Since bubble coalescence and breakup are neglected, n_b is constant in time.

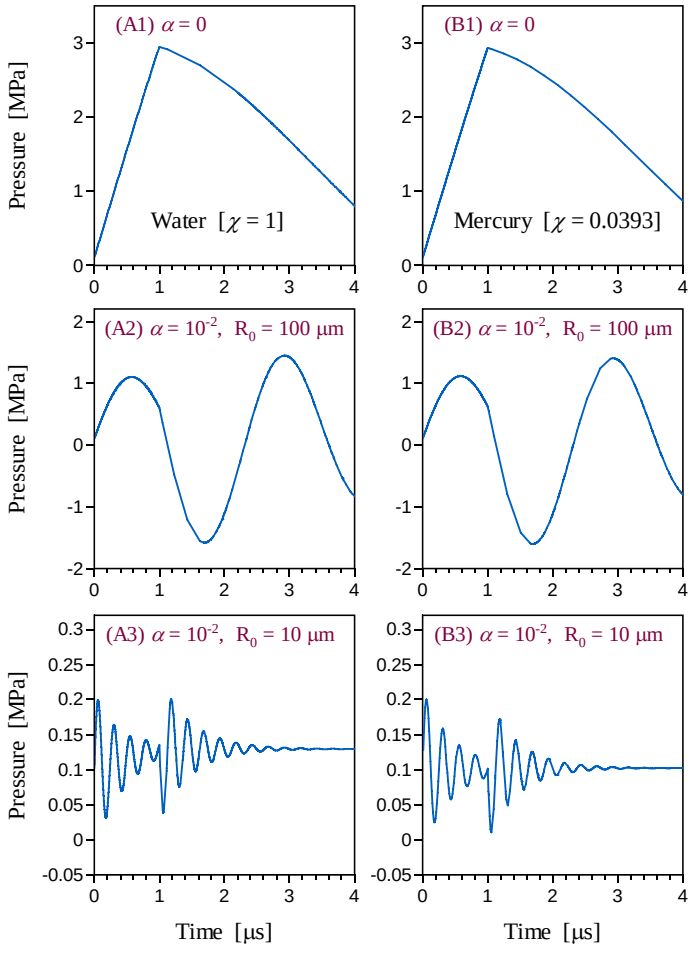

Fig. 2. Pressure-time curves at the cylinder center for (A) water and (B) mercury with different α and R_0.

The pressure-time curve for $\alpha = 0$ and $\chi = 1$ at the cylinder center ($r = 0$) is shown in Fig. 1(a), where α is the void fraction (gas volume/total volume) at $p = p_0$. For $t \le 1\,\mu$s, due to the heat input the pressure increases rapidly to a very high level [$\max(p) = 2.96$ MPa] and then decreases. The problematic pressure waves originate from

this dramatic pressure change. In Fig. 1(b), the pressure-time curve for mercury is shown for comparison, which was already presented in Ref. [4]. The pressure rise in mercury [$\max(p) = 72.1$ MPa] is observed to be much greater than that in water. This is mainly because the heat capacity of mercury is much smaller than that of water and mercury is thus more easily heated up. This is a difference between water and mercury. For fair comparison of the water and mercury cases with respect to pressure change, in the following we set $\chi = 0.0393$ in the case of mercury, holding χ for water unity. This setting allows us to obtain almost the same pressure rise in both liquids; see Figs. 2(A1) and 2(B1).

To elucidate the effect of bubbles in water, we performed computations for a finite α and different equilibrium radii of bubbles, R_0. Figures 2(A2) and 2(A3) show the pressure-time curves for water for $\alpha = 10^{-2}$ and two different R_0. In both cases, pressure oscillation is observed. As R_0 decreases, the maximum amplitude of the pressure oscillation decreases, that is, the bubbles get a stronger mitigation effect. For $R_0 = 10\,\mu$m, the amplitude is about 15 times smaller than that without bubbles. This is the same tendency as observed in mercury; see Figs. 2(B2) and 2(B3) for $\chi = 0.0393$ and Ref. [4] for $\chi = 1$. This dependence on bubble radius comes from the fact that bubbles' eigenfrequency depends on their radius.

Surprisingly, the frequency of the pressure oscillation in water is very close to that in mercury. This seems to be inconsistent with the previously mentioned fact that the eigenfrequency of individual bubbles in water is much different from that in mercury. Here we discuss the origin of this apparent inconsistency. It is known that pulsating bubbles emit pressure waves and interact with each other through these waves. Bubble-bubble interaction of this type changes the eigenfrequency of the bubbles [7–11]. The eigenfrequency of the present system is given by

$$\omega = \sqrt{\omega_0^2 + \frac{3\alpha c_L^2}{R_0^2}} \quad (\equiv \omega_b), \tag{7}$$

where

$$\omega_0 = \sqrt{\frac{3\kappa p_0 + (3\kappa - 1)2\sigma / R_0}{\rho R_0^2}} \tag{8}$$

is the (angular) eigenfrequency of the individual bubbles, c_L is the sound speed of the host liquid, and κ is the polytropic exponent of the gas.

From Eqs. (7) and (8), we found that $\psi^2 \gg \omega_0^2$ in the considered cases, where

$$\psi^2 \equiv \frac{3\alpha c_L^2}{R_0^2}. \tag{9}$$

This finding allows us to approximate ω_b as

$$\omega_b \approx \sqrt{\frac{3\alpha c_L^2}{R_0^2}}. \tag{10}$$

From this equation, we can find an interesting correspondence between water and mercury. Since the sound speed of water is almost equal to that of mercury, one finds that

$$\omega_{b,W} \approx \omega_{b,M} \tag{11}$$

for the same bubble condition (i.e., α and R_0); see Fig. 3, where $\omega_b / 2\pi$ in different conditions are shown. This means that bubbly water and bubbly mercury have almost the same eigenfrequency and they respond to pressure change in a similar fashion. This is consistent with the above numerical result and resolves the apparent inconsistency. What we have found here is a similarity of bubble clouds in water and mercury. This notable similarity would make water study useful in examining the mitigation effect of bubbles in mercury.

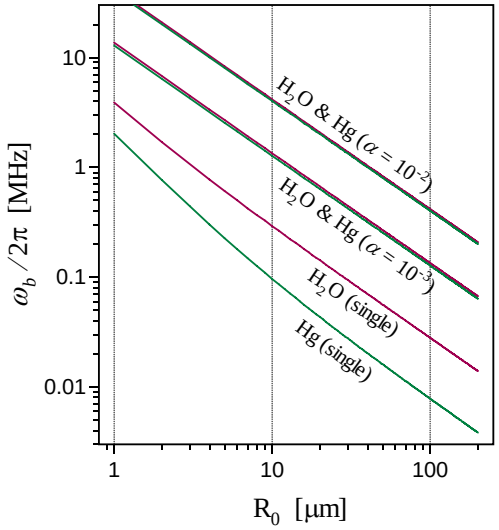

Fig. 3. $\omega_b / 2\pi$ in water and mercury in different conditions as functions of bubble radius. In single bubble cases (denoted by "single"), $\omega_b / 2\pi$ in water and mercury are significantly different from each other. However, for $\alpha = 10^{-3}$ or 10^{-2}, they are indistinguishable.

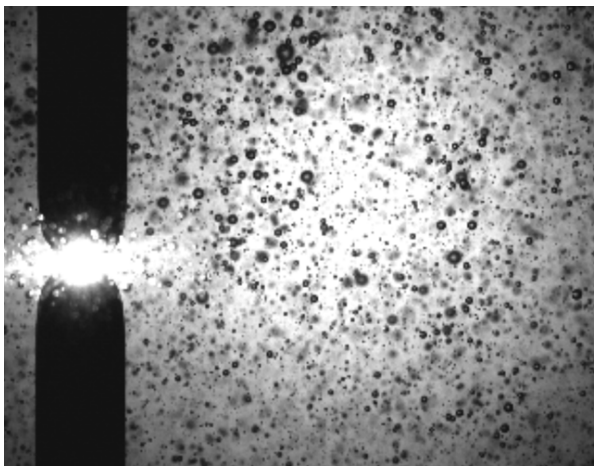

Fig. 4. High-speed photograph taken from the water experiment. When high-voltage spark occurs between the electrodes (the black bars), an intense pressure wave and a light pulse are emitted. Microbubbles (the black spheres) begin to pulsate when hit by the pressure wave.

3. Recent Water Experiment and Remaining Issues

Encouraged by the above theoretical findings, we recently performed a water experiment aiming at verifying the ability of microbubbles in a realistic condition. In this experiment, we used a swirl-type bubble generator which produces very small bubbles by a strongly swirling liquid flow. To generate intense pressure waves, we used electrodes; see Fig. 4. High-voltage sparks occurring between the electrodes generate pressure waves very similar to the proton-induced one. The left panel of Fig. 5 shows the measured acceleration imposed on a nearby channel wall. This clearly shows that the magnitude of acceleration decreases as the amount of injected gas increases. The right panel of Fig. 5 shows the maximum acceleration normalized by that for $\alpha = 0$ as a function of α. For $\alpha \geq 10^{-3}$, the maximum acceleration level is lower than 1/10 of the original: We have finally achieved a strong mitigation of pressure waves. This result of water study could indirectly confirm the ability of microbubbles in mercury through the theoretically found similarity. Details of this experiment will be presented elsewhere.

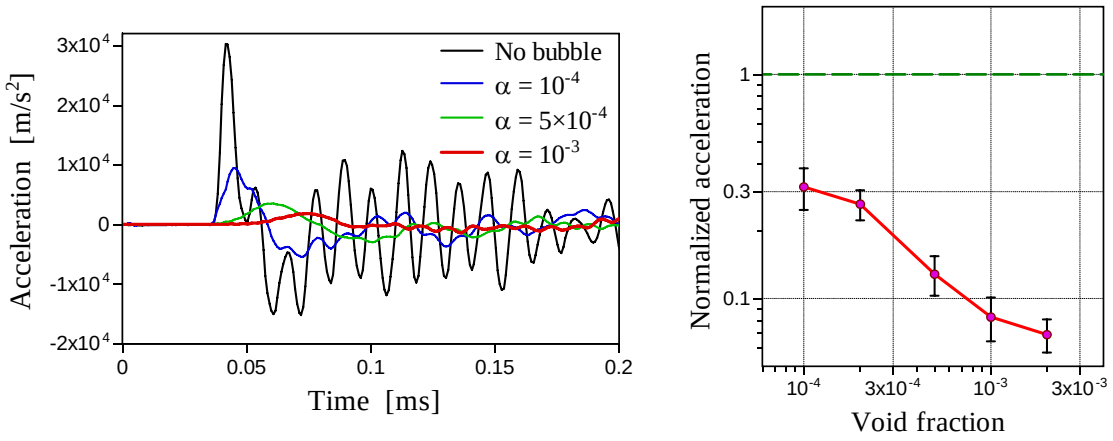

Fig. 5. (left) Acceleration-time curves for different α and (right) maximum acceleration normalized by that for $\alpha = 0$ as a function of α.

We have found a useful similarity between bubble clouds in mercury and water, which could make water study helpful. Also, we have succeeded to experimentally confirm the excellent ability of microbubbles to strongly damp intense pressure waves. However, we of course have to perform a mercury study to directly confirm the bubbles' effect in mercury and the validity of the theoretical predictions. We are now planning to perform an in-beam study using mercury and proton beams in collaboration with the SNS team. From this experiment, the excellent ability of microbubbles would be confirmed with mercury as well.

4. Acknowledgements

We would like to thank Prof. Y. Matsumoto and Dr. K. Okita for kindly supplying their DNS code. This work was partly supported by the Ministry of Education, Culture, Sports, Science, and Technology of Japan through a Grant-in-Aid for Young Scientists (B) (No. 20760122) and by the Japan Society for the Promotion of Science through a Grant-in-Aid for Scientific Research (B) (No. 20360090).

References

1. G. S. Bauer and H. Ullmaier, J. Nucl. Mater. **318** (2003) 26.
2. H. Soltner, Report ESS, 2004.
3. M. Ida, T. Naoe, and M. Futakawa, Phys. Rev. E **76** (2007) 046309.
4. K. Okita, S. Takagi, and Y. Matsumoto, J. Fluid Sci. Tech. **3** (2008) 116.
5. M. Ida, T. Naoe, and M. Futakawa, Nucl. Instr. Meth. Phys. Res. A **600** (2009) 367.
6. M. Ida, K. Haga, H. Kogawa, T. Naoe, and M. Futakawa, J. Phys. Soc. Jpn (2010), in press.
7. A. Shima, Trans. ASME, J. Basic Eng. **93** (1971) 426.
8. S. T. Zavtrak: Sov. Phys. Acoust. **33** (1987) 145.
9. M. Ida, Phys. Lett. A **297** (2002) 210.
10. M. Ida, J. Phys. Soc. Jpn. **71** (2002) 1217.
11. M. Ida, Phys. Fluids **17** (2005) 097107.